PREDICTION OF STIFFNESS FOR TOW-BASED DISCONTINUOUS COMPOSITES

Y. Li[1], S. Pimenta[1], M. Thierry[1], W. Y. Tan[1]

[1]meComposites, Department of Mechanical Engineering, Imperial College London,
South Kensington Campus, London, SW7 2AZ, UK
Email: yizhuo.li10@imperial.ac.uk

Keywords: Discontinuous composites, Stiffness field, Stochastic model, FE simulation

Abstract
Tow-based discontinuous composites are a new class of high-performance materials composed of carbon-fibre tows randomly oriented in a polymeric matrix. The discontinuous and random architecture of these materials implies that their local properties — including the stiffness — are highly inhomogeneous. Therefore, this work aims at developing a new model to predict the local stiffness field of tow-based discontinuous composites, while accounting for its intrinsic variability and implementing the method in a Finite Element environment. A multi-scale model based on a ply-by-ply laminate analogy is used to determine the stiffness of an equivalent laminate consisting of randomly-oriented and discontinuous plies. This model generates a distribution of stiffness values which are locally assigned to stiffness "seeds", mapped on the geometry of a component to be modelled using Finite Element simulations (in Abaqus). The FE model generates a heterogeneous strain field in the component, which shows good agreement with experimental observations on these materials. This model can be used to account for the variability in the mechanical properties of tow-based discontinuous composites when simulating structural components, thus contributing to a more sound design.

1. Introduction

Tow-based discontinuous composites (TBDCs) are a new class of high-performance materials composed of carbon-fibre tows randomly oriented in a polymeric matrix. This architecture allows TBDCs to achieve high fibre contents and to be mouldable through automated processes, thus combining the manufacturability of metals and the stiffness of quasi-isotropic continuous fibre composites [1].

The network of randomly arranged carbon-fibre tows implies that the stiffness of TBDCs is highly inhomogeneous; a large variability in the strain field under a uniform remote stress applied has been observed experimentally [2]. Therefore, to better predict the mechanical response of these materials in structural design, the variability in the local stiffness of TBDCs needs to be considered in Finite Element (FE) simulations.

This study proposes an analytical model coupled with FE simulations to predict and account for the variability in the stiffness of TBDCs in structural design. A multi-scale model, considering an equivalent ply-by-ply idealisation of the architecture of TBDCs (see Figure 1), is derived in Section 2; this model is used to predict the local stiffness fields of a TBDC structure, which are then implemented automatically in a FE model, as described in Section 3. The simulation results are compared to experimental findings and further discussed in Section 4, while Section 5 presents the main conclusions.

Excerpt from ISBN 978-3-00-053387-7

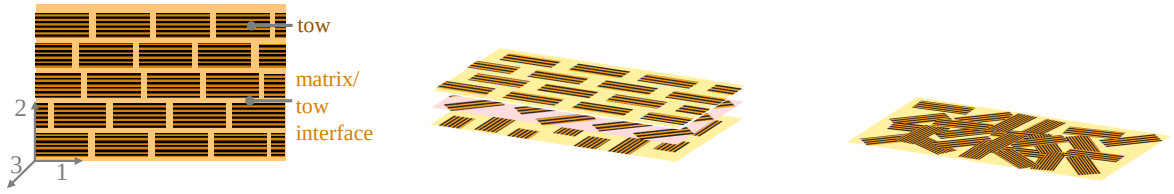

(a) UD discontinuous lamina (b) Equivalent laminate (c) Actual TBDC material

Figure 1. Multi-scale architecture of TBDCs used for modelling

2. Model development

2.1. Meso-scale (tow to lamina)

The model predicts the stiffness of TBDCs following a multi-scale approach (Figure 1). Focusing on the meso-scale (Figure 1 (a)), the stiffness of a UD discontinuous lamina (identified with 'l' in superscript) with tow volume fraction of 100% is calculated from the properties of the tows (identified with 't' in superscript) and the properties of the matrix (identified with 'm' in subscript). The tows are characterised by their geometry (tow length l^{t}, width w^{t} and thickness t^{t}) and elastic properties (stiffnesses E^{t}_{11}, E^{t}_{22}, shear moduli G^{t}_{12}, G^{t}_{23}, and Poisson's ratios ν^{t}_{12}, ν^{t}_{23}). The elastic properties of the matrix considered are its stiffness E_{m}, shear modulus G_{m}, and Poisson's ratio ν_{m}.

The longitudinal stiffness E^{l}_{11} of the laminate is determined from a shear-lag model [3] as:

$$E^{\mathrm{l}}_{11} = \frac{E^{\mathrm{t}}_{11}}{1 + \dfrac{1}{\lambda \cdot l_{\mathrm{char}} \cdot \tanh(\lambda \cdot l_{\mathrm{char}})}}, \tag{1}$$

where $\lambda = \sqrt{(2 \cdot G^{\mathrm{t}}_{12})/(t_{\mathrm{char}} \cdot t_{\mathrm{m}} \cdot E^{\mathrm{t}}_{11})}$, $l_{\mathrm{char}} = l^{\mathrm{t}}/8, t_{\mathrm{char}} = (w^{\mathrm{t}} \cdot t^{\mathrm{t}})/[2(w^{\mathrm{t}} + t^{\mathrm{t}})]$; and the embedded matrix thickness is $t_{\mathrm{m}} = (\sqrt{\pi/(4V_{\mathrm{f}})} - 1)\phi_{\mathrm{f}}$ (where ϕ_{f} is the fibre diameter and V_{f} is the fibre volume fraction, assuming a square packing of the fibres).

The laminate's transverse and shear moduli E^{l}_{22}, E^{l}_{33}, G^{l}_{12}, G^{l}_{13} and G^{l}_{23} can be obtained from the general expression from Halpin-Tsai [4] for a property P in direction i:

$$P^{\mathrm{l}}_i = P_{\mathrm{m}} \frac{1 + \eta_i \xi_i}{1 - \eta_i} \quad \text{with} \quad \eta_i = \frac{\frac{P^{\mathrm{t}}_i}{P_{\mathrm{m}}} - 1}{\frac{P^{\mathrm{t}}_i}{P_{\mathrm{m}}} + \xi_i}, \tag{2}$$

where the geometric coefficients are $\xi_{22} = 2(w^{\mathrm{t}}/t^{\mathrm{t}})$, $\xi_{33} = 2(t^{\mathrm{t}}/w^{\mathrm{t}})$, and $\xi_{12} = \xi_{13} = \xi_{23} = 1$, considering a rectangular cross-section of the tows.

The Poisson's ratio of the lamina are equal to that of the tows, considering the volume fraction of tows in the lamina is 100%.

2.2. Macro-scale (lamina to equivalent laminate)

Consider the equivalent laminate consisting of N UD discontinuous laminae (Figure 1 (b)), each with its own randomly assigned orientation θ_l, with $l = 1, 2, ..., N$. The stiffness matrix of a UD 0° lamina $\mathbf{C}_0$ is calculated from its elastic properties (from Section 2.1). For a lamina with an orientation of θ_l, its stiffness matrix $\mathbf{C}_{\theta_l}$ is determined by rotating $\mathbf{C}_0$ using a transformation matrix $\mathbf{T}(\theta_l)$ [5]. The

Excerpt from ISBN 978-3-00-053387-7

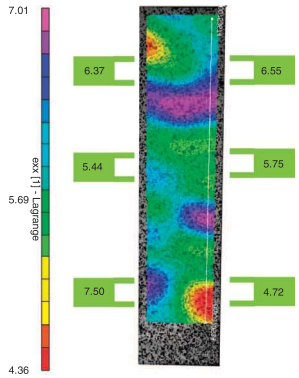

(a) The strain field of a TBDC specimen under uni-axial tensile stress. (The strains presented are measured in percentage)

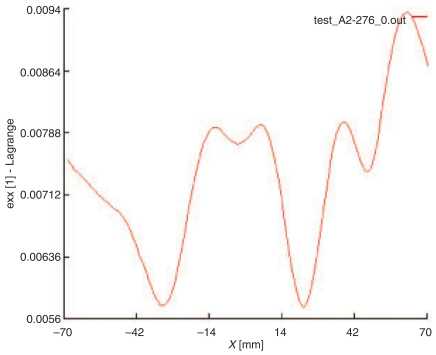

(b) Strain field along a path in the specimen in (a)

Figure 2. Strain field of TBDCs consisting of tows with 50.8 mm length and 8.4 mm width [2]

stiffness of the laminate with N randomly-oriented laminae is computed using Classical Laminate theory by averaging the stiffness matrix of each lamina as

$$\mathbf{C}_{\text{TBDC}} = \frac{\Sigma_{l=1}^{N} \mathbf{C}_{\theta_l}}{N}. \tag{3}$$

By repeating the random generation of orientation angles and the application of Eq. 3 for K realisations, a *statistical distribution* of the local stiffness values of a TBDC laminate can be generated.

Considering a given probability density function $f(\theta)$ for the distribution of tow orientations, Eq. 3 can be rewritten as

$$\mathbf{C}_{\text{TBDC}} = \int_0^{\pi} \mathbf{C}_{\theta} \cdot f(\theta) \cdot \mathrm{d}\theta, \tag{4}$$

to give a *deterministic* expected global stiffness of the TBDC laminate.

3. FE Implementation: generating representative stiffness fields

To better represent the TBDC material with its variability in local stiffness, a Finite Element (FE) model is built with Abaqus considering 3D shells under in-plane stress. This requires:

(a) Defining the characteristic size associated with the spatial variability of the stiffness of the material. Experimental observations (see Figure 2) show that major fluctuations in the strain field, and hence stiffness, occur with a spacing of approximately the tow width w^{t}. Consequently, *stiffness seeds* are created with corresponding spacing as shown in Figure 3 (a);

(b) Assigning a stiffness value to each stiffness seed: for a specimen consisting of K stiffness seeds, this implies running the stochastic model described in Section 2.2 for K realisations;

(c) Calculating the stiffness at each *integration point*: in the FE model, the stiffness value E_{ip} at an integration point is estimated from the stiffness of the n seeds in its neighbourhood (i.e. within a distance equal to the tow width w^{t}):

$$E_{\text{ip}} = \frac{\Sigma_{j=1}^{n} \frac{E_j}{r_j}}{\Sigma_{j=1}^{n} \frac{1}{r_j}}, \tag{5}$$

where r_j is the distance between the stiffness seed j and the integration point (with $r_j \leq w^{\text{t}}$).

Excerpt from ISBN 978-3-00-053387-7

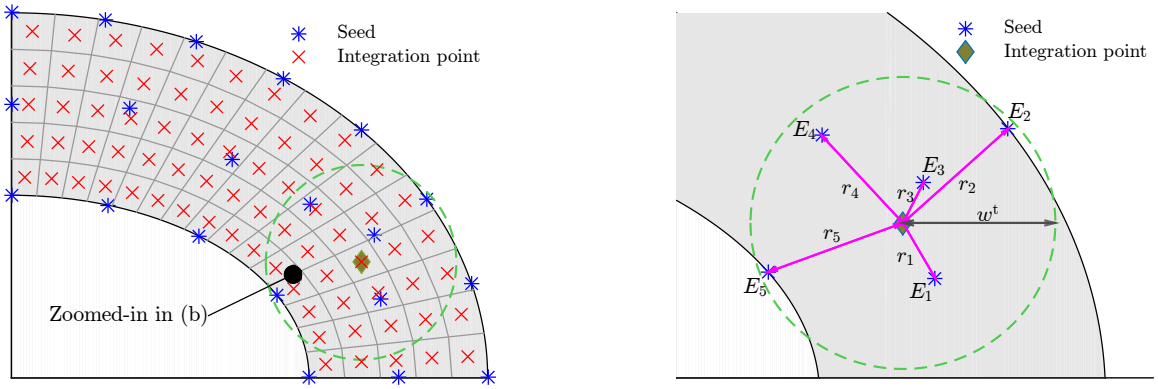

(a) Distribution of *seeds* and *integration points* in a part

(b) Mapping stiffness from seeds to integration points

Figure 3. Stiffness field distribution defined by seeds and integration points

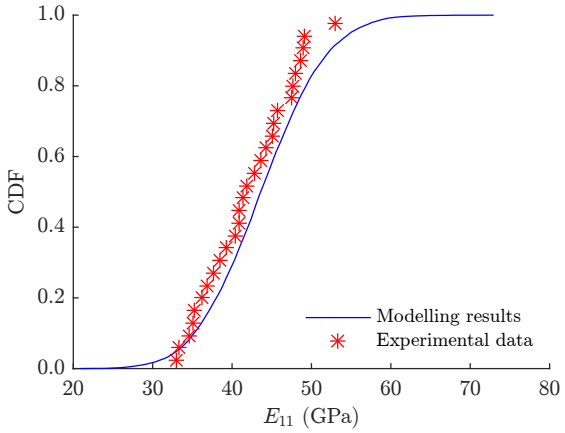

Figure 4. Comparison of experimental data and modelling results for the variability of stiffness

4. Results

4.1. Stiffness distributions and comparison against experimental data

The model described in Section 2 was implemented in Matlab and run for the inputs described in Table 1. Figure 4 shows the Cumulative Density Function (CDF) of the stiffness values by running the stochastic model for 10 000 realisations. The variability in the value of stiffness is well captured by the model compared to experimental data [2].

4.2. Stiffness field generated by FE simulation

Figure 5 shows the longitudinal strain field of a TBDC specimen with a length of 305 mm, a width of 38 mm, and a thickness of 4.3 mm, fixed on the left edge and subjected to a uniform displacement of 1 mm on the right edge; the results are generated from Abaqus, considering a varying local stiffness field in the specimen as described in Section 3. The strain field shows good qualitative agreement with that observed experimentally (Figure 2 (a) [2]).

Excerpt from ISBN 978-3-00-053387-7

Table 1. Inputs for the model (UD material properties considering V_f = 51.8%; with stiffness in GPa and dimensions in mm) [6]

E_{11}^t	E_{22}^t	E_m	G_{12}^t	G_{23}^t	G_m	ν_{12}^t	ν_{23}^t	ν_m	l^t	w^t	t^t
119	7.6	4.0	3.3	2.8	1.4	0.34	0.37	0.40	50.8	8.4	0.125

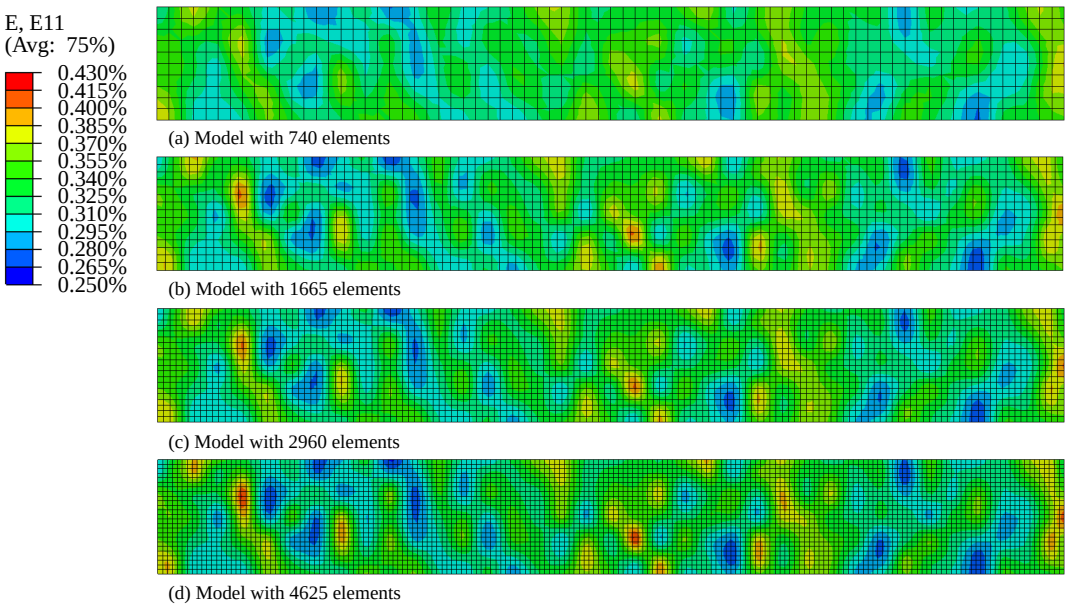

Figure 5. FE results for the strain field with varying local stiffness, considering different mesh sizes

Different mesh sizes were considered for the FE implementation and it is found that, when the elements are smaller than the characteristic distance between the stiffness seeds (equivalent to the tow width w^t), the results are independent of the mesh size considered.

5. Conclusions

The analytical model developed predicts the average stiffness of TBDCs and is able to capture the variability of stiffness in TBDCs, showing good agreement with experimental data.

The FE implementation of the stiffness model, considering a mapping between stiffness seeds and integration points, assures the mesh independence of the results, and generate a stiffness field that is similar to the pattern observed in experiments.

Acknowledgements

S. Pimenta acknowledges the support from the Royal Academy of Engineering in the scope of her Research Fellowship on *Multiscale discontinuous composites for large scale and sustainable structural applications* (2015-2019).

The authors also acknowledge S.K. Nothdurfter and K. Schuffenhauer (from the Advanced Composite Research Center of Lamborghini Automobili S.p.A.) for funding and several interesting discussions.

Excerpt from ISBN 978-3-00-053387-7

References

[1] S. Pimenta, A. Ahuja, and A. Yong. Damage tolerant tow-based discontious composites. In *Proc. 20th International Conference on Composite Materials*, 19-24 Jul 2015.

[2] P. Feraboli, E. Peitso, T. Cleveland, and P. B. Stickler. Modulus measurement for prepreg-based discontinuous carbon fiber/epoxy systems. *Journal of Composite Materials*, 43(19):1947–1965, 2009.

[3] S. Pimenta and P. Robinson. An analytical shear-lag model for brick-and-mortar composites considering non-linear matrix response and failure. *Composites Science and Technology*, 104:111–124, 2014.

[4] J. C. Halpin and J. L. Kardos. The Halpin-Tsai equations: a review. *Polymer Engineering and Science*, 16(5):344–352, 1976.

[5] S W Tsai and E M Wu. A general theory of strength for anisotropic materials. *Journal of Composite Materials*, 5:58–80, 1971.

[6] Torayca T700S data sheet. `http://www.toraycfa.com/pdfs/T700SDataSheet.pdf`. Accessed: 2016-04-06.

Excerpt from ISBN 978-3-00-053387-7